Chemistry of Metals and Alloys

Chem. Met. Alloys 16 (2023) 14-21
Ivan Franko National University of Lviv
http://publications.lnu.edu.ua/chemetal

The $SrO–Pr_2O_3–CoO$ system

Oksana ZAREMBA[1]*, Myroslava KURYLAS[1], Roman GLADYSHEVSKII[1]

[1] *Department of Inorganic Chemistry, Ivan Franko National University of Lviv, Kyryla i Mefodiya St. 6, 79005 Lviv, Ukraine*
* *Corresponding author. E-mail: oksana.zaremba@lnu.edu.com*

Received March 15, 2023; accepted June 29, 2023
https://doi.org/10.30970/cma16.0434

The phase diagram of the $SrO–Pr_2O_3–CoO$ system was constructed based on the results of X-ray diffraction of polycrystalline samples synthesized by solid-state reaction. Under the conditions of the experiment, the isothermal section contains 9 one-phase, 17 two-phase, and 9 three-phase regions. The formation of three substitutional solid solutions with extended homogeneity ranges was observed: $Sr_{1-x}Pr_xCoO_3$ with cubic perovskite-type structure ($CaTiO_3$, Pearson symbol *cP*5, space group *Pm*-3*m*), $Pr_{1-x}Sr_xCoO_3$ with orthorhombic perovskite-type structure ($GdFeO_3$, Pearson symbol *oP*20, space group *Pnma*), and $Sr_{2-x}Pr_xCoO_4$ (tetragonal Ruddlesden-Popper-type structure K_2NiF_4, Pearson symbol *tI*14, space group *I*4/*mmm*). The character of the interaction of the components in the $SrO–Pr_2O_3–CoO$ system is similar to that observed in the related system $SrO–Nd_2O_3–CoO$.

Oxides / Solid-state synthesis / X-ray diffraction / Phase diagram / Crystal structure

Introduction

Studies of *A*–*R*–*T*–O systems containing an alkaline-earth (*A*), a rare-earth (*R*), and a transition metal (*T*), and oxygen, are relevant due to the formation of compounds that (despite rather simple crystal structures) exhibit a wide range of attractive electrical and magnetic characteristics and are promising materials for practical applications [1-3]. Analysis of literature data on four-component compounds in the $SrO–R_2O_3–CoO$ systems indicated the formation of $Sr_{1-x}R_xCoO_3$ phases for all of the rare-earth metals, except Pm and Lu [4]. However, the phases differ in terms of crystal structure and Sr/*R* ratio, which was a motivation for a more detailed study.

Numerous phases with 1:1:3 stoichiometry belong to the perovskite family. The aristotype of this broad structure family is the cubic $CaTiO_3$ type. In the literature this structure is often called cubic or ideal (undeformed) perovskite [5,6], since the mineral itself has a distorted structure. Ideal perovskite consists of a three-dimensional framework of regular $[TiO_6]$ octahedra connected by vertices; the calcium atoms are placed in the cuboctahedral voids formed between the octahedra (Fig. 1). The ideal cubic structure has a number of derivatives that are produced by deformation of the structure and, accordingly, are characterized by lower symmetry. One of the most common derivatives is the $GdFeO_3$ type, which is orthorhombic [7] (Fig. 2). It arises due to mismatch between the size of the (*A*,*R*) atoms and the size of the cuboctahedral void (the *A*,*R* atoms are too small). Thanks to the deformation, the coordination polyhedron around the (*A*,*R*) atom transforms from a cuboctohedron (coordination number CN = 12) to a square antiprism (CN = 8), while the coordination polyhedron around the *T* atom remains an octahedron $[TO_6]$.

In the $SrO–R_2O_3–CoO$ systems the formation of a $Sr_{2-x}R_xCoO_4$ substitutional solid solutions with a tetragonal Ruddlesden-Popper-type structure K_2NiF_4 has also been observed [8]. For the large atoms (K) the coordination environment can be described as a one-capped square antiprism (or three-capped trigonal prism) of fluorine atoms $[KF_9]$, while for the smaller cations (Ni) the coordination polyhedron is an octahedron $[NiF_6]$ (Fig. 3).

A literature search showed that phase diagrams have been constructed only for the $SrO–R_2O_3–CoO$ systems where *R* is La, Nd, Sm, and Gd [9]. The aim of the present work was to establish the existence of four-component phases in the $SrO–Pr_2O_3–CoO$ system, to study their crystal structures and to build the corresponding phase equilibria.

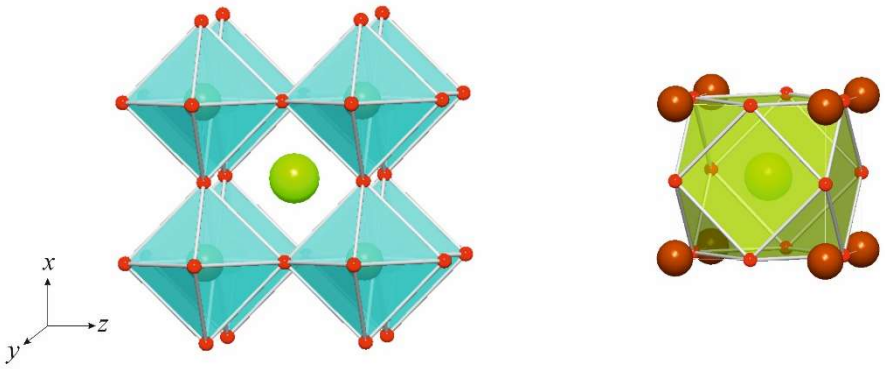

Fig. 1 The structure type $CaTiO_3$ and coordination polyhedra around Ca (cuboctahedron) and Ti (octahedron) atoms.

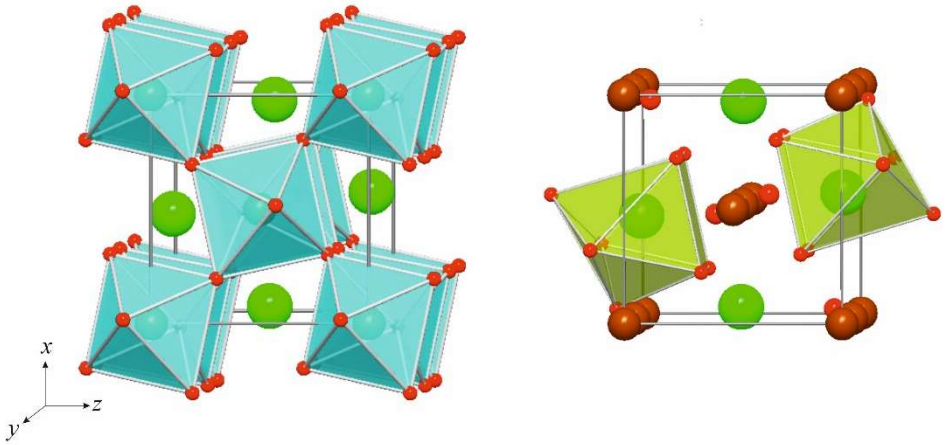

Fig. 2 The structure type $GdFeO_3$ and coordination polyhedra around Gd (tetragonal antiprism) and Fe (octahedron) atoms.

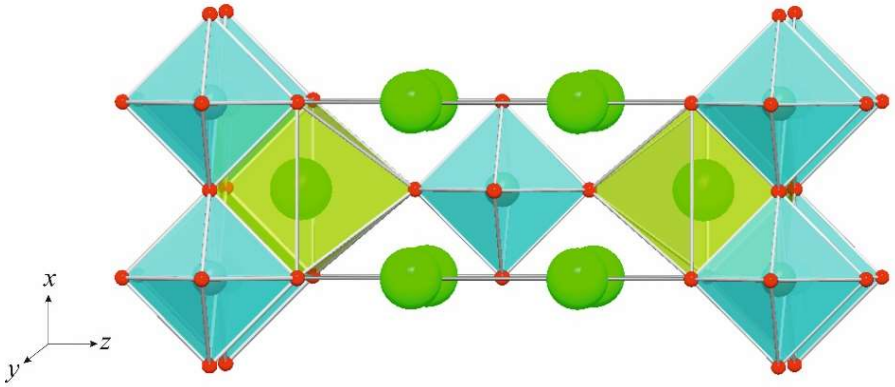

Fig. 3 The structure type K_2NiF_4 and coordination polyhedra around K (one-capped square antiprism) and Ni (octahedron) atoms.

Experimental details

The synthesis of polycrystalline samples was carried out by solid-state reaction in two stages. High-purity powders of strontium and cobalt carbonates and rare-earth metal oxides were used as reagents. Firstly, the initial components were weighed, mixed and ground in an agate mortar for 5 min manually. Then, the homogeneous mixtures were heated in corundum crucibles for 24 h at 1000°C under air in a muffle furnace, in order to decompose the carbonates. The degree of decomposition was monitored by weighing the mixtures before and after heating (more than 99 mass %). Finally, the obtained mixtures were ground again, pressed into pellets (the weight of a pellet was ~0.5 g) and sintered under air for 8 h at 1200°C in a tube furnace. The change in color of the pellets after sintering (compared to the mixtures of the starting materials), as well as the hardness and brittleness of the samples after sintering, indicated that solid-phase reactions had occurred. X-ray powder diffraction data for phase and structural analyses were collected on a DRON-2.0 M diffractometer (Fe $K\alpha$ radiation, 2θ range 20-80°). The structures were refined by the Rietveld method (DBWS program [10]). The refinements, which included refinement of the cell parameters, atomic coordinates and site occupancies, were evaluated by the Bragg reliability factor R_B.

Results and discussion

The investigation was started from the synthesis and analysis of polycrystalline samples with the nominal composition $Sr_{0.5}R_{0.5}CoO_3$, where R is a rare-earth metal, in order to establish the existence of four-component perovskites in the $SrO–R_2O_3–CoO$ systems. The results of the phase analysis based on X-ray powder diffraction are presented in Table 1. It was revealed that perovskite phases of approximate composition $Sr_{0.5}R_{0.5}CoO_3$ form in the systems where R = Pr, Nd, Sm, Eu, Gd, and Tb. No deviation from the ideal cubic perovskite type ($CaTiO_3$, Pearson symbol *cP*5, space group *Pm*-3*m*) was detected. The refined compositions and cell parameters of these phases are given in Table 2. The cell parameters decrease when going from Pr to Tb, but the change is not linear, which is due to the different Sr/R ratios in the phases.

The samples of composition $Sr_{0.5}R_{0.5}CoO_3$ where R is Dy, Ho, Er, Tm, Yb, or Lu, turned out to be three-phase, containing in equilibrium R_2O_3, CoO, and a quaternary phase with cubic perovskite-type structure ($CaTiO_3$), which can be assumed to be the limiting composition of a solid solution based on cubic $SrCoO_3$ ([4]). The cell parameters of the perovskite phase increase when going from Dy to Lu, which is caused by a gradual change in the Sr/R ratio (Table 3).

To study the interaction of the components in the $SrO–Pr_2O_3–CoO$ system, 24 four-component polycrystalline samples were synthesized and investigated. The phase analysis based on X-ray diffraction (Table 4), showed that the initial Pr_2O_3 reagent was oxidized to Pr_7O_{12}, while the SrO phase was mainly observed in the form of $Sr(OH)_2(H_2O)$ hydrate. The phase diagram of the $SrO–Pr_2O_3–CoO$ system, obtained under the conditions of our study, is presented in Fig. 4. As can be seen from the figure, 9 single-phase, 17 two-phase, and 9 three-phase regions exist. We did not observe a two-phase region between two perovskite phases along the isoconcentrate of 50 mol.% CoO (dashed lines), but a composition-induced polymorphic transformation from the cubic $CaTiO_3$- to the orthorhombic $GdFeO_3$-type structure takes place when increasing the Pr content. It may be noted that the character of the interaction of the components in the $SrO–Pr_2O_3–CoO$ system (studied at 1200°C) is very similar to that earlier observed for the $SrO–Nd_2O_3–CoO$ system (isothermal section constructed at 1100°C [9]). In the boundary $SrO–Pr_2O_3$ system we confirmed the formation of a single compound, Sr_2PrO_4, which crystallizes with own structure type and has the following crystallographic characteristics: Pearson symbol *oP*14, space group *Pbam*, a = 0.6125(1), b = 1.0287(1), c = 0.3591(1) nm. The compound $PrCoO_3$ with $GdFeO_3$-type structure was observed in the boundary $Pr_2O_3–CoO$ system: Pearson symbol *oP*20, space group *Pnma*, a = 0.5390(2), b = 0.7599(3), c = 0.5359(2) nm. Two compounds were confirmed in the boundary SrO–CoO system: $Sr_6Co_5O_{15}$ ($Ba_6Ni_5O_{15}$-type structure, Pearson symbol *hR*78, space group *R*32, a = 0.9431(3), c = 1.2660(5) nm) and $Sr_3Co_2O_6$ (own structure type, Pearson symbol *oI*68, space group *Immm*, a = 0.3827(1), b = 1.1463(2), c = 2.0074(3) nm), however, we did not observe any compound at the composition $SrCoO_3$ under the conditions used here. In the $SrO–Pr_2O_3–CoO$ system the formation of three substitutional solid solutions characterized by extended homogeneity ranges, was revealed: $Sr_{1-x}Pr_xCoO_3$ with the cubic perovskite structure type $CaTiO_3$ (Pearson symbol *cP*5, space group *Pm*-3*m*), $Pr_{1-x}Sr_xCoO_3$ with the orthorhombic perovskite structure type $GdFeO_3$ (Pearson symbol *oP*20, space group *Pnma*), and $Sr_{2-x}Pr_xCoO_4$ with the structure type K_2NiF_4 (Pearson symbol *tI*14, space group *I*4/*mmm*). Refined cell parameters within the solid solutions are presented in Tables 5-7. For both four-component phases with $CaTiO_3$- and $GdFeO_3$-type structures, there is a tendency to an increase of the cell volume with increasing strontium content. For the phase with the structure type K_2NiF_4 a decrease of the a-parameter and an increase of the c-parameter was observed under similar conditions. The diffraction patterns of single-phase samples within the solid solutions are shown in Figs. 5-7.

Table 1 Results of the phase analysis of polycrystalline samples with nominal composition $Sr_{0.5}R_{0.5}CoO_3$.

No	Nominal composition	Phase composition	Structure type	Pearson symbol	Space group	Content, mass %
1	$Sr_{0.5}Pr_{0.5}CoO_3$	$Sr_{0.5}Pr_{0.5}CoO_3$	$CaTiO_3$	*cP*5	*Pm*-3*m*	100
2	$Sr_{0.5}Nd_{0.5}CoO_3$	$Sr_{0.5}Nd_{0.5}CoO_3$	$CaTiO_3$	*cP*5	*Pm*-3*m*	100
3	$Sr_{0.5}Sm_{0.5}CoO_3$	$Sr_{0.5}Sm_{0.5}CoO_3$	$CaTiO_3$	*cP*5	*Pm*-3*m*	100
4	$Sr_{0.5}Eu_{0.5}CoO_3$	$Sr_{0.5}Eu_{0.5}CoO_3$	$CaTiO_3$	*cP*5	*Pm*-3*m*	94.1
		CoO	NaCl	*cF*8	*Fm*-3*m*	5.9
5	$Sr_{0.5}Gd_{0.5}CoO_3$	$Sr_{0.5}Gd_{0.5}CoO_3$	$CaTiO_3$	*cP*5	*Pm*-3*m*	93.0
		$SrCoO_3$	$SrZrO_3$	*tI*20	*I*4/*mcm*	7.0
6	$Sr_{0.5}Tb_{0.5}CoO_3$	$Sr_{0.5}Tb_{0.5}CoO_3$	$CaTiO_3$	*cP*5	*Pm*-3*m*	92.3
		Tb_2O_3	$(Mn_{0.5}Fe_{0.5})_2O_3$	*cI*80	*Ia*-3	7.7
7	$Sr_{0.5}Dy_{0.5}CoO_3$	$Sr_{1-x}Dy_xCoO_3$	$CaTiO_3$	*cP*5	*Pm*-3*m*	72.0
		Dy_2O_3	$(Mn_{0.5}Fe_{0.5})_2O_3$	*cI*80	*Ia*-3	20.0
		CoO	NaCl	*cF*8	*Fm*-3*m*	8.0
8	$Sr_{0.5}Ho_{0.5}CoO_3$	$Sr_{1-x}Ho_xCoO_3$	$CaTiO_3$	*cP*5	*Pm*-3*m*	65.5
		Ho_2O_3	$(Mn_{0.5}Fe_{0.5})_2O_3$	*cI*80	*Ia*-3	24.2
		CoO	NaCl	*cF*8	*Fm*-3*m*	10.3
9	$Sr_{0.5}Er_{0.5}CoO_3$	$Sr_{1-x}Er_xCoO_3$	$CaTiO_3$	*cP*5	*Pm*-3*m*	59.2
		Er_2O_3	$(Mn_{0.5}Fe_{0.5})_2O_3$	*cI*80	*Ia*-3	29.6
		CoO	NaCl	*cF*8	*Fm*-3*m*	11.2
10	$Sr_{0.5}Tm_{0.5}CoO_3$	$Sr_{1-x}Tm_xCoO_3$	$CaTiO_3$	*cP*5	*Pm*-3*m*	53.6
		Tm_2O_3	$(Mn_{0.5}Fe_{0.5})_2O_3$	*cI*80	*Ia*-3	34.0
		CoO	NaCl	*cF*8	*Fm*-3*m*	12.4
11	$Sr_{0.5}Yb_{0.5}CoO_3$	$Sr_{1-x}Yb_xCoO_3$	$CaTiO_3$	*cP*5	*Pm*-3*m*	53.3
		Yb_2O_3	$(Mn_{0.5}Fe_{0.5})_2O_3$	*cI*80	*Ia*-3	32.8
		CoO	NaCl	*cF*8	*Fm*-3*m*	13.9
12	$Sr_{0.5}Lu_{0.5}CoO_3$	$Sr_{1-x}Lu_xCoO_3$	$CaTiO_3$	*cP*5	*Pm*-3*m*	57.3
		Lu_2O_3	$(Mn_{0.5}Fe_{0.5})_2O_3$	*cI*80	*Ia*-3	28.2
		CoO	NaCl	*cF*8	*Fm*-3*m*	14.5

Table 2 Refined composition and cell parameters of $Sr_{0.5}R_{0.5}CoO_3$ perovskites ($CaTiO_3$ structure type, Pearson symbol *cP*5, space group *Pm*-3*m*).

No	Composition	*a*, nm	R_B
1	$Sr_{0.54(3)}Pr_{0.46(3)}CoO_3$	0.38249(6)	0.099
2	$Sr_{0.39(3)}Nd_{0.61(3)}CoO_3$	0.38177(5)	0.073
3	$Sr_{0.44(2)}Sm_{0.56(2)}CoO_3$	0.38072(3)	0.055
4	$Sr_{0.59(2)}Eu_{0.41(2)}CoO_3$	0.38115(5)	0.065
5	$Sr_{0.55(2)}Gd_{0.45(2)}CoO_3$	0.38005(4)	0.084
6	$Sr_{0.52(2)}Tb_{0.48(2)}CoO_3$	0.38030(5)	0.064

Table 3 Refined composition and cell parameters at the *R*-rich boundary of cubic perovskite-type solid solutions ($CaTiO_3$ structure type, Pearson symbol *cP*5, space group *Pm*-3*m*).

No	Composition	*a*, nm	R_B
1	$Sr_{0.61(2)}Dy_{0.39(2)}CoO_3$	0.38156(3)	0.061
2	$Sr_{0.69(2)}Ho_{0.31(2)}CoO_3$	0.38203(4)	0.062
3	$Sr_{0.74(2)}Er_{0.26(2)}CoO_3$	0.38308(3)	0.066
4	$Sr_{0.81(2)}Tm_{0.19(2)}CoO_3$	0.38381(2)	0.065
5	$Sr_{0.86(2)}Yb_{0.14(2)}CoO_3$	0.38420(2)	0.052
6	$Sr_{0.88(2)}Lu_{0.12(2)}CoO_3$	0.38476(3)	0.057

Table 4 Phase analysis of polycrystalline samples of the $SrO–Pr_2O_3–CoO$ system.

No	Nominal composition ($SrO:1/2Pr_2O_3:CoO$), mol. %	Phase composition	Structure type	Pearson symbol	Space group	Content, mass %
1	10:30:60	$Pr_{1-x}Sr_xCoO_3$	$GdFeO_3$	*oP*20	*Pnma*	84.1
		CoO	NaCl	*cF*8	*Fm*-3*m*	15.9
2	20:20:60	$Sr_{1-x}Pr_xCoO_3$	$CaTiO_3$	*cP*5	*Pm*-3*m*	85.2
		CoO	NaCl	*cF*8	*Fm*-3*m*	14.8
3	30:10:60	$Sr_{1-x}Pr_xCoO_3$	$CaTiO_3$	*cP*5	*Pm*-3*m*	81.7
		CoO	NaCl	*cF*8	*Fm*-3*m*	18.3
4	5:45:50	$Pr_{1-x}Sr_xCoO_3$	$GdFeO_3$	*oP*20	*Pnma*	100
5	10:40:50	$Pr_{1-x}Sr_xCoO_3$	$GdFeO_3$	*oP*20	*Pnma*	100
6	15:35:50	$Pr_{1-x}Sr_xCoO_3$	$GdFeO_3$	*oP*20	*Pnma*	100
7	20:30:50	$Pr_{1-x}Sr_xCoO_3$	$GdFeO_3$	*oP*20	*Pnma*	100
8	25:25:50	$Sr_{1-x}Pr_xCoO_3$	$CaTiO_3$	*cP*5	*Pm*-3*m*	100
9	30:20:50	$Sr_{1-x}Pr_xCoO_3$	$CaTiO_3$	*cP*5	*Pm*-3*m*	100
10	35:15:50	$Sr_{1-x}Pr_xCoO_3$	$CaTiO_3$	*cP*5	*Pm*-3*m*	100
11	40:10:50	$Sr_{1-x}Pr_xCoO_3$	$CaTiO_3$	*cP*5	*Pm*-3*m*	100
12	45:5:50	$Sr_6Co_5O_{15}$	$Ba_6Ni_5O_{15}$	*hR*78	*R*32	~58
		$Sr_{1-x}Pr_xCoO_3$	$CaTiO_3$	*cP*5	*Pm*-3*m*	~42
13	20:40:40	$Pr_{1-x}Sr_xCoO_3$	$GdFeO_3$	*oP*20	*Pnma*	67.1
		$Sr_{2-x}Pr_xCoO_4$	K_2NiF_4	*tI*14	*I*4/*mmm*	32.9
14	35:25:40	$Sr_{2-x}Pr_xCoO_4$	K_2NiF_4	*tI*14	*I*4/*mmm*	64.5
		$Sr_{1-x}Pr_xCoO_3$	$CaTiO_3$	*cP*5	*Pm*-3*m*	35.5
15	50:10:40	$Sr_3Co_2O_6$	$Sr_3Co_2O_6$	*oI*68	*Immm*	~75
		$Sr_{2-x}Pr_xCoO_4$	K_2NiF_4	*tI*14	*I*4/*mmm*	~25
16	20:46.7:33.3	$Sr_{2-x}Pr_xCoO_4$	K_2NiF_4	*tI*14	*I*4/*mmm*	100
17	30:36.7:33.3	$Sr_{2-x}Pr_xCoO_4$	K_2NiF_4	*tI*14	*I*4/*mmm*	100
18	40:26.7:33.3	$Sr_{2-x}Pr_xCoO_4$	K_2NiF_4	*tI*14	*I*4/*mmm*	100
19	10:60:30	$PrCoO_3$	$GdFeO_3$	*oP*20	*Pnma*	38.5
		$Sr_{2-x}Pr_xCoO_4$	K_2NiF_4	*tI*14	*I*4/*mmm*	31.6
		Pr_7O_{12}	Pr_7O_{12}	*hR*57	*R*-3	29.9
20	50:20:30	$Sr_{2-x}Pr_xCoO_4$	K_2NiF_4	*tI*14	*I*4/*mmm*	~85
		$Sr(OH)_2(H_2O)$	$Sr(OH)_2(H_2O)$	*oP*8	$Pmc2_1$	~15
21	60:10:30	$Sr_{2-x}Pr_xCoO_4$	K_2NiF_4	*tI*14	*I*4/*mmm*	40.9
		$Sr(OH)_2(H_2O)$	$Sr(OH)_2(H_2O)$	*oP*8	$Pmc2_1$	16.0
		SrO	NaCl	*cF*8	*Fm*-3*m*	5.0
		$Sr_3Co_2O_6$	$Sr_3Co_2O_6$	*oI*68	*Immm*	38.1
22	20:60:20	$Sr_{2-x}Pr_xCoO_4$	K_2NiF_4	*tI*14	*I*4/*mmm*	63.0
		Pr_7O_{12}	Pr_7O_{12}	*hR*57	*R*-3	37.0
23	40:40:20	$Sr_{2-x}Pr_xCoO_4$	K_2NiF_4	*tI*14	*I*4/*mmm*	63.0
		Sr_2PrO_4	Sr_2PbO_4	*oP*14	*Pbam*	29.2
		Pr_7O_{12}	Pr_7O_{12}	*hR*57	*R*-3	7.8
24	60:20:20	$Sr_{2-x}Pr_xCoO_4$	K_2NiF_4	*tI*14	*I*4/*mmm*	60.1
		$Sr(OH)_2(H_2O)$	$Sr(OH)_2(H_2O)$	*oP*8	$Pmc2_1$	37.4
		Sr_2PrO_4	Sr_2PbO_4	*oP*14	*Pbam*	2.5

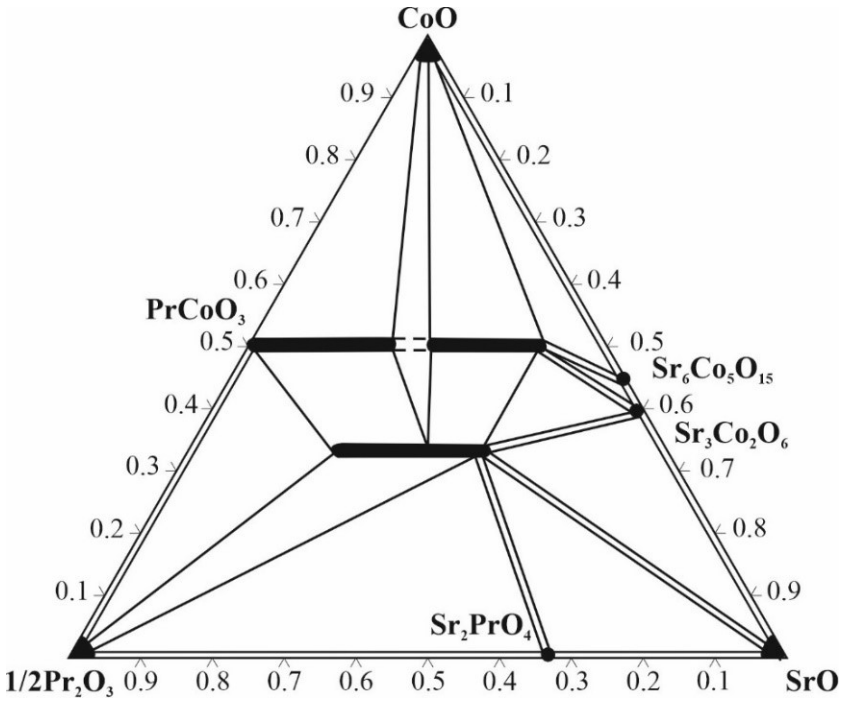

Fig. 4 Phase diagram of the SrO–Pr_2O_3–CoO system from this investigation.

Table 5 Refined cell parameters within the solid solution (Sr,Pr)CoO_3 with cubic perovskite structure ($CaTiO_3$ structure type, Pearson symbol *cP*5, space group *Pm*-3*m*).

No	Nominal composition (SrO:1/2Pr_2O_3:CoO), mol. %	*a*, nm	*V*, nm^3	R_B
1	25:25:50	0.38249(6)	0.05596	0.097
2	30:20:50	0.38226(3)	0.05586	0.081
3	35:15:50	0.38272(3)	0.05606	0.095
4	40:10:50	0.38376(3)	0.05652	0.083

Table 6 Refined cell parameters within the solid solution (Sr,Pr)CoO_3 with orthorhombic perovskite structure ($GdFeO_3$ structure type, Pearson symbol *oP*20, space group *Pnma*).

No	Nominal composition (SrO:1/2Pr_2O_3:CoO), mol. %	*a*, nm	*b*, nm	*c*, nm	*V*, nm^3	R_B
1	5:45:50	0.54012(7)	0.76035(14)	0.53627(7)	0.22024	0.097
2	10:40:50	0.53690(7)	0.76042(12)	0.54183(7)	0.22121	0.135
3	15:35:50	0.53739(7)	0.76046(12)	0.54290(7)	0.22186	0.231
4	20:30:50	0.53826(5)	0.76055(9)	0.54391(6)	0.22266	0.089

Table 7 Refined cell parameters within the solid solution $(Sr,Pr)_2CoO_4$ (K_2NiF_4 structure type, Pearson symbol *tI*14, space group *I*4/*mmm*).

No	Nominal composition (SrO:1/2Pr_2O_3:CoO), mol. %	*a*, nm	*c*, nm	*V*, nm^3	R_B
1	20:46.7:33.3	0.38039(3)	1.2332(1)	0.17844	0.099
2	30:36.7:33.3	0.37850(4)	1.2359(1)	0.17706	0.120
3	40:26.7:33.3	0.37833(5)	1.2434(1)	0.17797	0.157

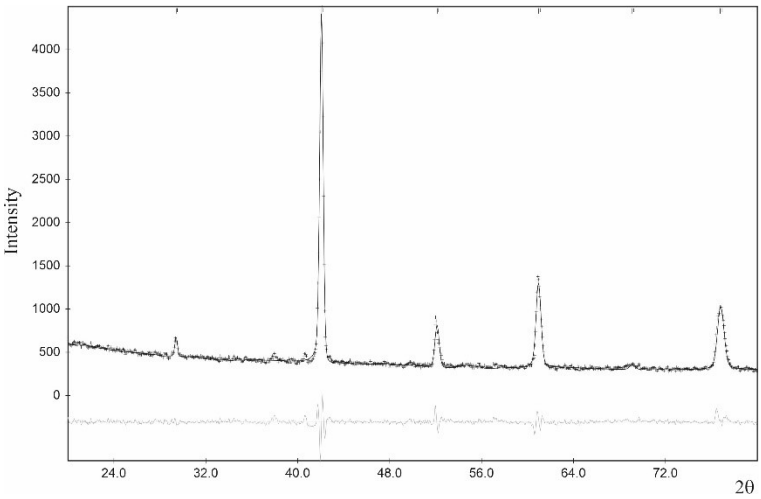

Fig. 5 Diffraction pattern of a single-phase sample of $Sr_{0.5}Pr_{0.5}CoO_3$ cubic perovskite (sample composition 25 mol.% SrO : 25 mol.% 1/2Pr_2O_3 : 50 mol.% CoO).

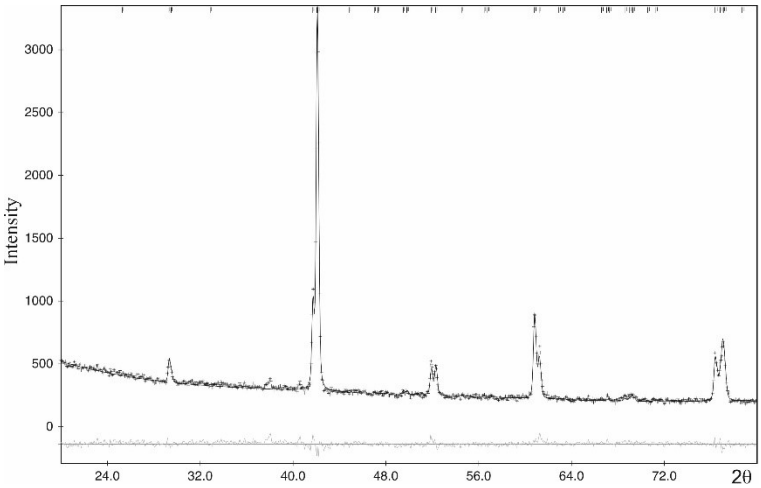

Fig. 6 Diffraction pattern of a single-phase sample of $Sr_{0.4}Pr_{0.6}CoO_3$ orthorhombic perovskite (sample composition 20 mol.% SrO : 30 mol.% 1/2Pr_2O_3 : 50 mol.% CoO).

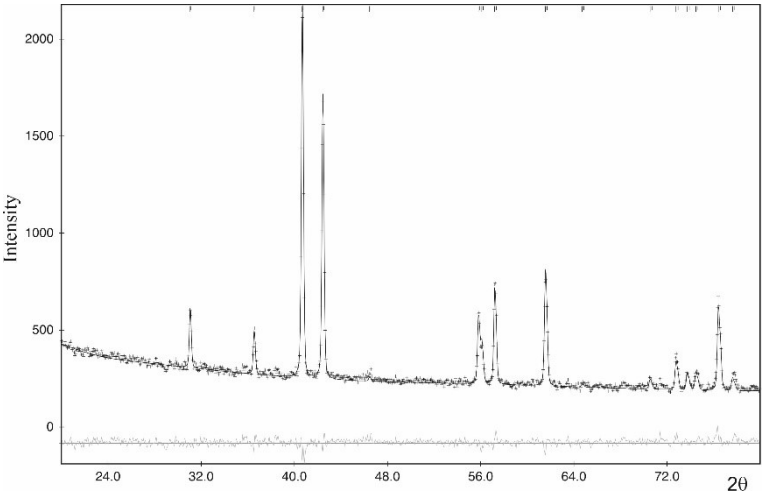

Fig. 7 Diffraction pattern of a single-phase sample of $Sr_{2-x}Pr_xCoO_4$ (sample composition 30 mol. % SrO : 36.7 mol. % 1/2Pr_2O_3 : 33.3 mol. % CoO).

Summary

The experiment was started from the synthesis and investigation of polycrystalline samples with nominal composition $Sr_{0.5}R_{0.5}CoO_3$, where *R* is a rare-earth metal. Under the conditions of our experiment the existence of four-component perovskites $Sr_{0.5}R_{0.5}CoO_3$ with cubic perovskite-type structure ($CaTiO_3$ type, Pearson symbol *cP*5, space group *Pm*-3*m*) was established for the light rare-earth metals (*R* = Pr, Nd, Sm, Eu, Gd, and Tb). The samples with heavy rare-earth metals (*R* = Dy, Ho, Er, Tm, Yb, and Lu) contained in equilibrium the corresponding R_2O_3 oxide, CoO, and a quaternary phase with cubic perovskite structure, presumably the boundary of a solid solution based on $SrCoO_3$.

The interaction of the components in the $SrO–Pr_2O_3–CoO$ system was studied based on X-ray diffraction of 24 ceramic polycrystalline samples, synthesized by a two-stage solid-state reaction method, starting from $SrCO_3$, Pr_2O_3, and $CoCO_3$. Final heating was performed at 1200°C for 8 h. The existence of three extended homogeneity regions was revealed: $Pr_{1-x}Sr_xCoO_3$ with orthorhombic perovskite type ($GdFeO_3$), $Sr_{1-x}Pr_xCoO_3$ with cubic perovskite type ($CaTiO_3$), and $Sr_{2-x}Pr_xCoO_4$ with tetragonal type K_2NiF_4. The formation of Sr_2PrO_4 (own structure type, Pearson symbol *oP*14, space group *Pbam*), $PrCoO_3$ ($GdFeO_3$ structure type, Pearson symbol *oP*20, space group *Pnma*), $Sr_6Co_5O_{15}$ ($Ba_6Ni_5O_{15}$ structure type, Pearson symbol *hR*78, space group *R*32), and $Sr_3Co_2O_6$ (own structure type, Pearson symbol *oI*68, space group *Immm*) phases was confirmed in the boundary systems. An approximately isothermal section of the phase diagram of the $SrO–Pr_2O_3–CoO$ system under the conditions of our investigation was constructed in the full concentration range. It contains 9 one-phase, 17 two-phase and 9 three-phase regions.

References

[1] P. Wagner, *Phys. Status Solidi A*. 214 (2017) 1700394. https://doi.org/10.1002/pssa.201700394

[2] R.J.D. Tilley, *Perovskites Structure–Property Relationships*, John Wiley & Sons, Ltd., UK, 2016.

[3] S. Thomas, A. Thankappan, *Perovskite photovoltaics. Basic to Advanced Concepts and Implementation*, Academic Press, Elsevier, UK, 2018.

[4] P. Villars, K. Cenzual (Eds.), *Pearson's Crystal Data – Crystal Structure Database for Inorganic Compounds*, ASM International, Materials Park, OH, USA.

[5] R. Sondena, S. Stolen, P. Ravindran, T. Grande, N.L. Allan, *Phys. Rev. B*. 75 (2007) 184105-10. https://doi.org/10.1103/PhysRevB.75.184105

[6] M. Yashima, R. Ali, *Solid State Ionics* 180 (2009) 120-126. https://doi.org/10.1016/j.ssi.2008.11.019

[7] N.L. Ross, J. Zhao, R.J. Angel, *Solid State Chem.* 177 (2004) 3768-3775. https://doi.org/10.1016/j.jssc.2004.07.002

[8] S.K. Yeh, S.Y. Wu, C.S. Lee, Y. Wang, *Acta Crystallogr. B* 49 (1993) 806-811. https://doi.org/10.1107/S0108768193003246

[9] *Phase Equilibria Diagrams Database*, ACS and NIST, Westerville, OH, USA.

[10] D.B. Wiles, A. Sakthivel, R.A. Young, *Program DBWS3.2 for Rietveld Analysis of X-Ray and Neutron Powder Diffraction Patterns*, School of Physics, Georgia Institute of Technology, Atlanta, 1998.